Proposal of a machining test to evaluate dynamic synchronization error of rotary and linear axes with reversal of rotation direction

Qingzhao Li[1], Soichi Ibaraki[2], Wei Wang[3]

1. School of Mechanical and Electrical Engineering, University of Electronic Science and Technology of China, Chengdu 611731, China. Email: qingzhaoli@std.uestc.edu.cn
2. Department of Mechanical Systems Engineering, Hiroshima University, Hiroshima, 739-8527, Japan. Emai: ibaraki@hiroshima-u.ac.jp
3. School of Mechanical and Electrical Engineering, University of Electronic Science and Technology of China, Chengdu 611731, China. Email: wangwhit@163.com

ABSTRACT: The five-axis machining of a free-form surface often contains the reversal of a rotary axis' rotation direction with linear axis synchronized with it. This paper proposes a new machining test to quantitatively evaluate the influence of the reversal of rotation direction on the surface geometry and roughness. In the five-axis machining, the trajectory of tool position and orientation is firstly given in the workpiece coordinate system by the CAM (Computer-aided Manufacturing) software, and the CNC (Computerized Numerical Control) system converts it to the machine coordinate system to calculate command trajectories. This paper clarifies that the tool path smoothing in the machine coordinate system can potentially cause a large contour error because of the dynamic synchronization error of rotary and linear axes. Although some academic works in the literature presented the smoothing in the workpiece coordinate system, many commercial CNC systems still employ the smoothing in the machine coordinate system, partly because machine tool users or makers do not clearly see how significant this influence can be on the machining accuracy. The proposed machining test enables a user to quantitatively evaluate it. The machining experiment shows that the geometric error of the finished test piece was as large as 0.16 mm under the conventional smoothing in a commercial CNC system, which can be significantly larger than the influence of other typical geometric errors of a five-axis machine tool. This paper shows, by numerical simulation, that the smoothing in the workpiece coordinate system can completely eliminate this contour error.

Keywords: five-axis machining; tool path smoothing; contour error; machining test.

1. Introduction

Five-axis machine tools can tilt a tool or a workpiece by two rotary axes, which makes it widely used to process parts with complicated geometry in modern aerospace, and die and mold industries. To date, many measurement methods have been developed to test the geometric errors of five-axis machine tools [1], but there are few studies focusing on the test of machine tool dynamic performance. To measure the dynamic positioning error of the tool with respect to the worktable on a five-axis machine, ISO 10791-6 [2] presented schemes to measure the displacement of a precision sphere, attached to

the spindle, by a displacement sensor(s) installed on a worktable, e.g. the double ball bar tests [3] and the R-Test [4]. Due to the limited measurable range of the displacement sensor, this scheme requires the displacement of the tool-side sphere is nominally zero with respect to the worktable. Actual machining always has the relative displacement between the tool and the workpiece. Some researchers applied the standardized workpieces like the cone frustum [5] and S test piece [6] to test the dynamic performance of machine tools. The acceleration and deceleration in tool path smoothing can cause undesired contour errors and vibrations. For example, a part of the S-curve machining test piece is machined near the singularity of the five-axis kinematics, where rotary and linear axes are driven abruptly in an unstable manner. This part is often subject to a “scratch”-shaped geometric error of significant depth. It is clearly due to dynamic synchronous error of rotary and linear axes but no previous works have discussed its explicit cause. Cripps [7] designed a machining test performed under ball end milling and showed that the machining error caused by the drastic change of acceleration at machining singularity cannot be ignored.

This paper has two major original contributions. First, this paper proposes a new machining test to evaluate the dynamic synchronization error of rotary and linear axes with the reversal of rotation direction. In the experiment presented in Section 3, the finished test piece shows a significantly large step-shaped geometric error as large as 0.16 mm. Then, as the second contribution, this paper discusses its major cause.

In generating a tool path for a numerically controlled (NC) machine tool, most computer-aided manufacturing (CAM) software approximates the tool path by a series of linear segments to generate machining commands. Since the adjacent linear segments are only G0 continuous (position continuous), to avoid infinite acceleration at the transition point of linear segments, the smoothing of feedrate transition is indispensable. This paper clarifies that, on a five-axis machine, the smoothing can cause much larger contouring error due to an error in the synchronization of rotary and linear axes. Many commercial CNC systems employ the following procedure to calculate the command trajectory of each linear and rotary axis:

1) A position trajectory of tool center point (TCP), as well as its orientation trajectory, is given in the workpiece coordinate system (WCS) by e.g. CAM software as an NC program.

2) It is converted to the machine coordinates system (MCS) by solving the inverse kinematic problem to calculate the command trajectory for each linear and rotary axis.

3) Then each command trajectory is smoothed by applying a smoothing filter.

In this paper, the MCS represents the fixed coordinate system aligned with the machine’s linear axes. The WCS is a coordinate system attached to the rotary table, rotated with rotary axes. In commercial CNC systems, this smoothing is typically done by filtering the command profile with a FIR (Finite Impulse Response) filter, resulting in e.g. a trapezoidal

or S-curve velocity profile [8]. Such a FIR filtering inevitably introduces the delay to the command profile. For the interpolation of linear axes, it has been well known that this delay causes a contour error at corners. To improve the contour error at corners, the corner geometry is smoothed by parametrically fitting with higher-order curves. Erkorkmaz and Altintas [9] smoothed the tool path using the fitting of quintic spline. Sencer [10] designed the quintic Bezier blends with six control points to blend the discrete linear segments with curvature continuous transitions. Essid [11] and Rymansaib [12] used the high-order polynomials to describe the velocity profile to generate the tool path. Chen [13], Altintas [14], and Tajima [15] used the shaping filters to smooth the tool path at corners by reasonably tuning the dynamic parameters of the filters. The non-stop interpolation for feedrate scheduling was proposed that can also smooth the corner transition [16, 17]. These academic works presented the smoothing of corner transition for linear axes only.

In recent years, some researchers presented a smoothing scheme at corners under five-axis operations, and they contain the smoothing in the WCS instead of the smoothing in the MCS as described above. Sencer [18] converted the feedrate along the tool path in a cubic B-spline form in the WCS, and generated the tool path profile based on the spline expression of the feedrate considering the physical constraints of drives. Huang [19] proposed a novel curve “airthoid” to smooth the five-axis tool path in the WCS. Hu [20] smoothed the transition corners of the TCP in the WCS by G3 continuous PH lines. Jiang [21] proposed a decoupled five-axis local tool path smoothing method in the WCS by FIR filtering. Tajima [22] presented real-time interpolation in the WCS that synchronized translational and rotational motion of the tool using FIR filtering.

Although these academic works presented the smoothing in the WCS, commercial CNC systems still perform the smoothing in the MCS. The coordinate transformation performed on the CNC (step 2 above) is called the TCP (Tool Center Point) function. Many CNC systems have this function as an additional function to conventional three-axis control, and this is one reason why the smoothing is kept in the MCS. In our view, another potential reason is that machine tool users or makers do not clearly see how significant this influence can be on the machining accuracy. The machining test proposed in this paper clearly shows that the smoothing of linear and rotary axes can cause a large contour error.

The remained structure of this paper is as follows. A machining test with reversal of rotation direction is designed in the Section 2. The experiment of the machining test is made in Section 3. The analysis of the step-shaped contour error caused by the conventional smoothing, the proposal of improved tool path smoothing method, and the corresponding simulation validation are presented in Section 4. Final conclusion is drawn in Section 5.

2. Proposed machining test

Design principle in the proposed machining test: For easy measurement and analysis, the proposed machining test nominally makes a flat surface and its straightness is to be evaluated. The tool path in the WCS is a straight line that requires three axes motion (*X*-, *Y*- and *C*-axis). A reversal motion of *C*-axis is introduced at the middle position of the tool path. The proposed test piece geometry is designed such that the synchronization error of the tool position, with respect to the workpiece, in the radial direction of *C*-axis is copied onto the geometry of the finished surface when the *C*-axis reverses its rotation direction. The tool path and the reference trajectories of the axes are shown in Fig. 1.

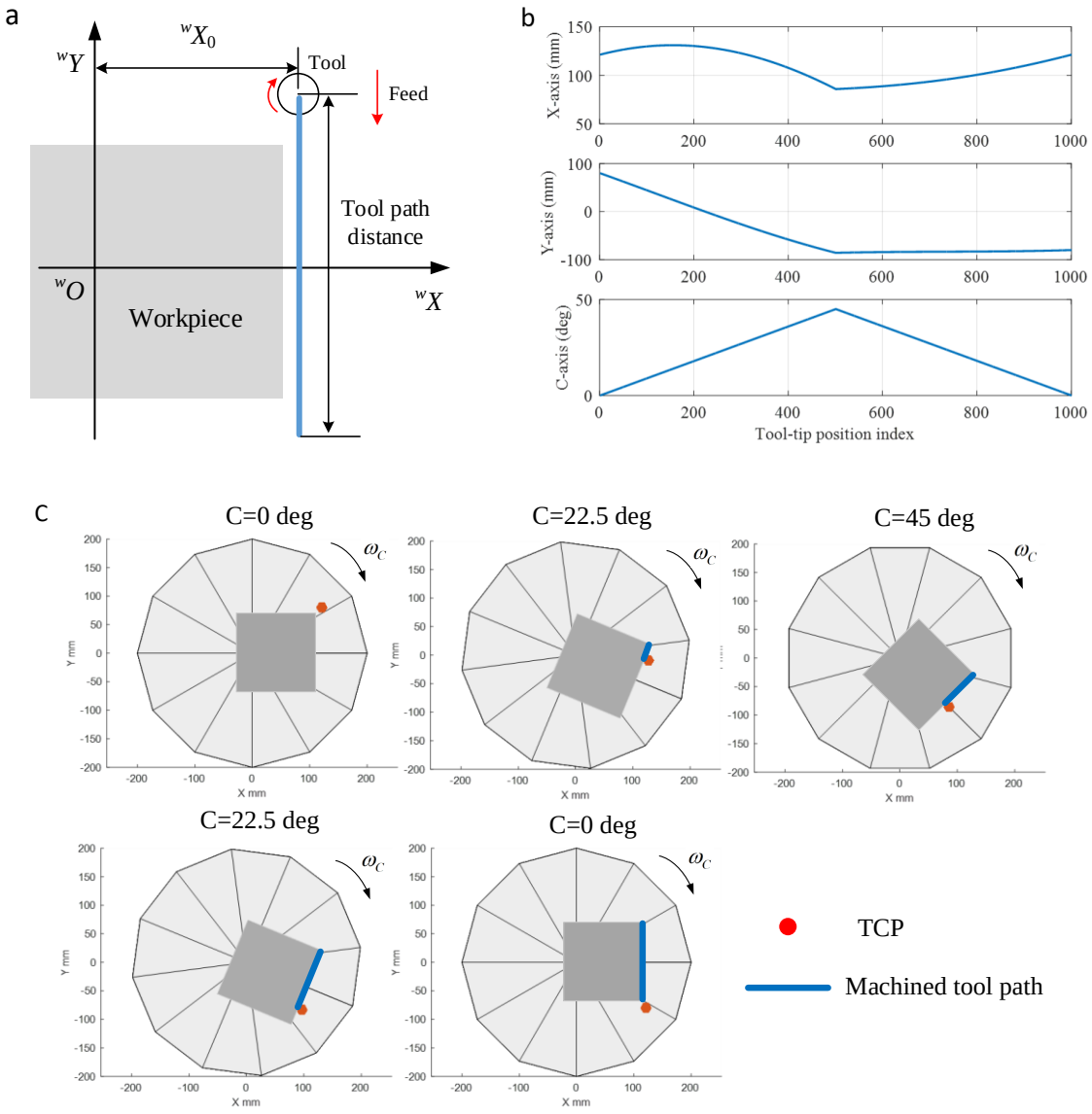

Fig. 1 Tool path in WCS and MCS in the proposed machining test (a) Tool path in WCS, (b) Reference trajectories in MCS, (c) Tool path in MCS.

In the WCS, the tool path lies in the XY plane and feeds in the Y direction. The tool path is symmetric about ^wX-axis and has an offset, $^wX_0$, relative to ^wY-axis. The key for this tool path is that *C*-axis is set from 0° to 45° in the first half of

the tool path and from 45° to 0° in the second half of the tool path. As shown in Fig. 1b, at the middle position of the designed tool path, the reference trajectories of all these three axes have a reversal motion which will lead to the acceleration change. The NC program should be written in the WCS, and uses the TCP control function of the CNC system. The feedrate of the tool in the WCS is constant at F. The tool position and orientation trajectories in the WCS are given by:

$$\begin{cases} {}^{w}X(j) = {}^{w}X_0 \\ {}^{w}Y(j) = F \cdot t \\ {}^{r}C(j) = \begin{cases} \omega_c \cdot t & , \quad {}^{r}C(j) < 45\text{deg} \\ -\omega_c \cdot t & , \quad {}^{r}C(j) \geq 45\text{deg} \end{cases} \end{cases} , \tag{1}$$

where ${}^{w}X_0$ is constant. Throughout this paper, the left-hand side superscript "r" represents a vector in the MCS, and "w" represents a vector in the WCS.

Remark: The proposed machining test is a general one. The typical reversal movement of C-axis can be replaced by A- or B-axis, and the corresponding synchronized moving axes should be Y-, Z-axis and X-, Z-axis. The rotary axis position can also be redefined to meet special test requirement.

3. Experiment

The machining test is conducted on a vertical five-axis machining center of the configuration shown in Fig. 2, NMV3000DCG by DMG Mori Co., Ltd., with the CNC system 30i by Fanuc Corp. In this paper, the MCS is defined as the fixed coordinate system with its orientation shown in Fig. 2. Its origin is at the nominal intersection of the B- and C-axis of rotation. The WCS is defined as a coordinate system attached to the rotary table, rotated with B- and C-axes. Its origin is also at the intersection of the B- and C-axis. When B=C=0°, it coincides with the MCS.

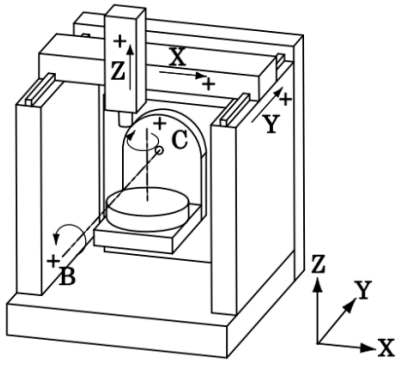

Fig. 2 Five-axis machine tool configuration.

In five-axis operations, the TCP trajectory in the WCS defines the geometry of the machined workpiece. Thus, typically, the CAM software generates the reference trajectory of the TCP position in the WCS, denoted by [${}^{w}X(j)$, ${}^{w}Y(j)$, ${}^{w}Z(j)$] (j=1, ..., N), as well as the tool orientation around X-, Y-, and Z-axes in the WCS, denoted by [${}^{w}I(j)$, ${}^{w}J(j)$, ${}^{w}K(j)$]. When these trajectories are sent to the CNC system in the form of an NC program (G-codes), the CNC system calculates the reference angular position trajectories for rotary axes, denoted by ${}^{r}B(j)$ and ${}^{r}C(j)$, by solving the inverse kinematic problem. Then, the reference trajectories for X-, Y-, and Z-axes are calculated by converting [${}^{w}X(j)$, ${}^{w}Y(j)$, ${}^{w}Z(j)$] to the MCS by the following equations:

$$\begin{cases} {}^{r}X(j) = {}^{w}X(j)\cos\left({}^{r}B(j)\right)\cos\left({}^{r}C(j)\right) + {}^{w}Y(j)\cos\left({}^{r}B(j)\right)\sin\left({}^{r}C(j)\right) \\ {}^{r}Y(j) = -{}^{w}X(j)\sin\left({}^{r}C(j)\right) + {}^{w}Y(j)\cos\left({}^{r}C(j)\right) \\ {}^{r}\mathrm{Z}(j) = {}^{w}\mathrm{Z}(j) + L\cos\left({}^{r}B(j)\right) \end{cases}, \tag{2}$$

where L represents the length of tool.

The geometry of the tool path, shown in Fig. 1a. is given by: ${}^{w}X_0$ 121.286 mm and the tool path distance 160 mm. The sampling time is set as 0.001 s. The feed rate in the WCS is set to 9180, 7120 and 3060 mm/min corresponding to the feed per tooth 0.102, 0.237 and 0.306 mm, which makes the angular velocity of C-axis 4500, 3490.20 and 1500 deg/min. The feed rate is set to be large in order to easily observe the influence of the dynamic error of the machine on the machining test. The specific machining conditions are listed in Table 1. Throughout the finishing process, the position profiles of X-, Y-, and C-axes, measured by linear or rotary encoder and fed back to the CNC system, were logged to an external PC by using the software, Servoguide by Fanuc. The setup is shown in Fig. 3.

Table 1 Machining conditions for experiment

Machining conditions	Workpiece	Tool	Cutting fluid	Axial depth of cut	Radial depth of cut	Feedrate in WCS	Spindle speed
Parameters	Aluminum alloy JIS A5052	Solid carbide radius end mill, DLC-PKE by OSG, Φ10×R1.0, 3 edgs	Oil mist	10 mm	0.2 mm	3060, 7120, 9180 mm/min	10000 r/min

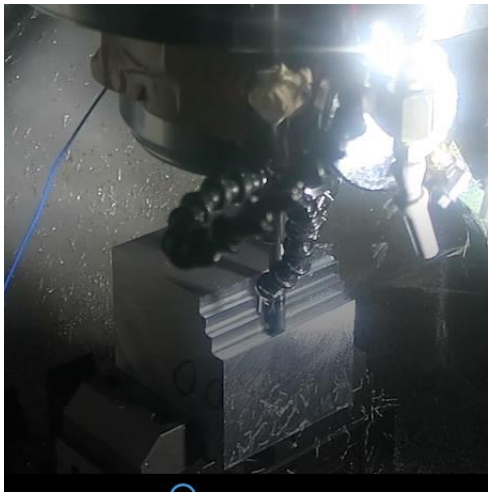

Fig. 3 Machining test setup.

The machining test was done under three feedrates in the WCS, F=3060, 7120, 9180 mm/min. The three faces at different heights in Fig. 3 were machined at different feedrates. The position trajectory of each axis, measured by linear encoders and recorded by Servoguide, is shown in Fig. 4a. The tool trajectory in the WCS, calculated by converting the trajectories in Fig. 4a into the WCS by inversely solving Eq. (2), is shown Fig. 4b. The *X*-position of the reference trajectory (dashed line) in the WCS is 121.286 mm but is shown as zero in Fig. 4b. Figure 4b shows that the contour error was at maximum 0.16 mm under the feedrate 9180 mm/min. This is calculated by the position profiles measured by linear encoders, and thus does not contain the influence of the machine's geometric errors, e.g. the position error of the *C*-axis of rotation or linear positioning or straightness error motions of linear axes. There is a small size fluctuation in the first half tool path, which is caused by the backlash of the X-axis. Because the machining test is used to evaluate the dynamic error of the machine, the fluctuation caused by the backlash will not be discussed in this paper.

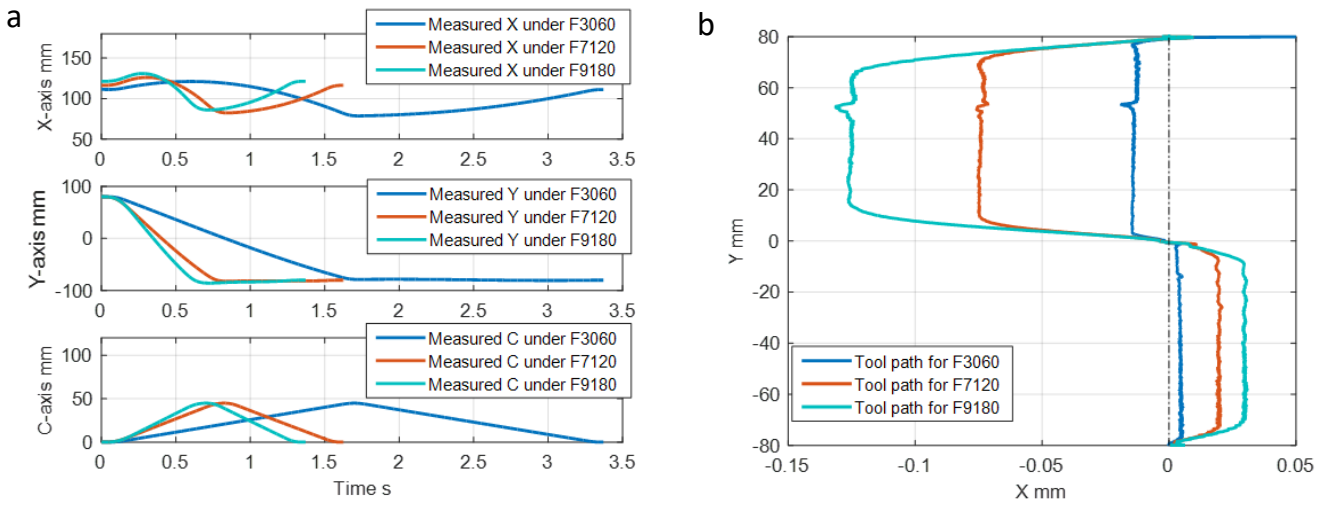

Fig. 4 Recorded *X*, *Y* and *C*-axis trajectories measured by linear encoders (a) measured trajectories in MCS, (b) tool paths converted to the WCS.

The geometric error of the machined surfaces under different feedrates was measured by the interferometry-based laser displacement sensor, SI-F10 by Keyence Corp (measuring resolution: 1 nm, linearity: ±0.2 μm, measurable range: 0.05 to 1.0 mm). The setup for the measurement is shown in Fig. 5. The laser displacement sensor was installed on the machine spindle. Without unclamping the finished test piece after the machining test, it was indexed by *C*- and *B*-axes such that the finished surfaces are nominally parallel to the machine's XY plane. Then, the finished surfaces were scanned by feeding the spindle to the Y direction at various X positions. Only 1) the straightness error motion of the Y-axis in the Z-direction over the feed travel (160 mm), and 2) the straightness error motion of the X-axis in the Z-direction over the measured range (10mm) influence the measurement. Compared to the measured geometric error of the finished test piece, the contributions of the machine's error motions 1) and 2), as well as the uncertainty of the laser displacement sensor, are negligibly small.

The measured geometries of the finished surfaces are shown in Fig. 6. The finished surfaces show a step of the size up to 0.14 mm at the feedrate F9180 mm/min in Fig. 6c. The profiles in Fig. 4b and 6 are very similar. It shows that the geometric error of the finished surfaces, shown in Fig. 6, is mostly caused by the dynamic error in the MCS, which is much larger than the influence of other error sources, e.g. the machine's geometric errors.

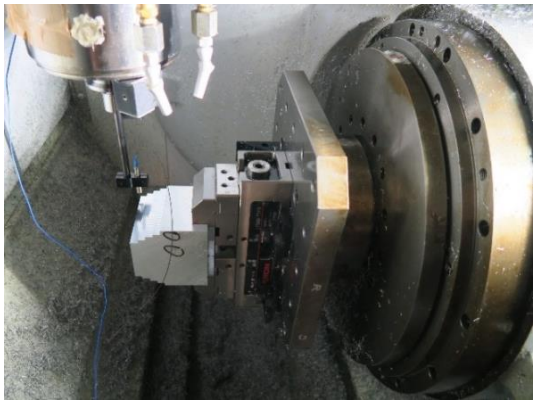

Fig. 5 Measurement of workpiece

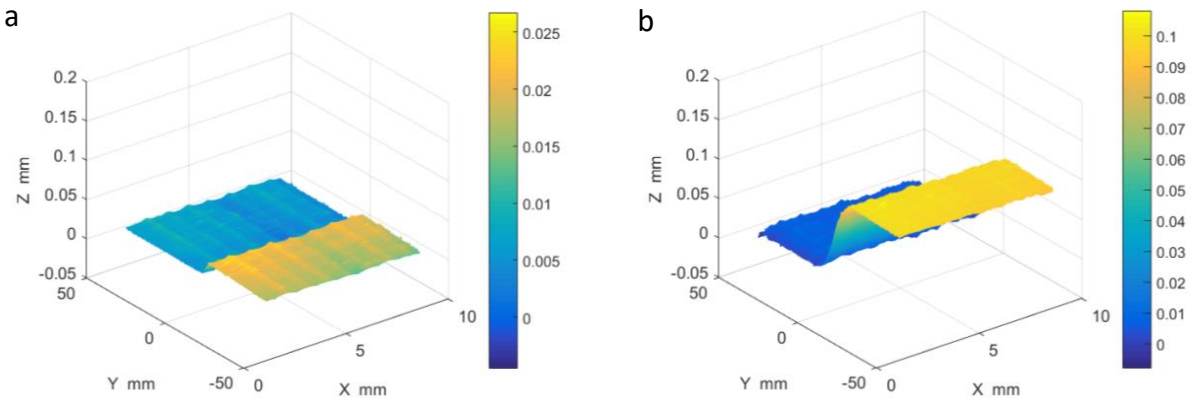

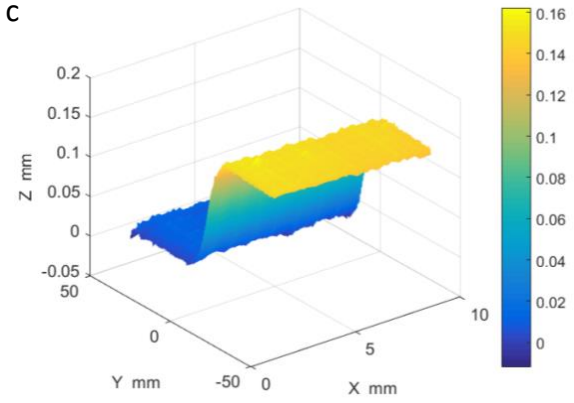

Fig. 6 Machined geometries of the finished surfaces (a) machined under the feedrate F3060, (b) machined under the feedrate F7120, (c) machined under the feedrate F9180.

4. Causes for step-shaped machining error

As shown in Fig. 4b and Fig. 6, there is a step-shaped machining error for the surfaces of the test piece. As illustrated in Section 3, the tool path shown in Fig. 4b is calculated by the position profiles measured by linear encoders, and thus does not contain the influence of the machine's geometric errors. The measured machining error in Fig. 6 is very similar to the profiles shown in Fig. 4b, which shows that the machining error is mostly affected by the dynamic error of the machine tool. The key for this proposed machining test is that there is a reversal movement for both the rotary and linear axes. Therefore, in this section, the causes for the step-shaped machining error of the designed test piece is analyzed based on the dynamic synchronization error caused by tool path smoothing.

4.1 Conventional tool path smoothing method

When the reference trajectory is given for each linear and rotary axis, it should be smoothed to ensure that its velocity, acceleration and jerk is within the permissible range, and to avoid undesired vibrations. In many commercial CNC systems, the Finite Impulse Response (FIR) filters are employed as online acceleration and deceleration (Acc/dec) processor to generate the reference trajectories with smoothed profiles. FIR filters are utilized to realize the well-known "trapezoidal acceleration" profile trajectories for high speed motions. The transfer function of a first order FIR filter defined in Laplace (s) domain is shown as below [15]:

$$M_i(s) = \frac{1}{T_i}\frac{1-e^{-sT_i}}{s}, \quad i = 1,2,\cdots,n \quad , \tag{3}$$

where T_i denotes the time constant of the *i*th FIR filter. When a velocity pulse is convolved with the FIR filter, the filtered output will increase the order because of the integrator 1/*s* and be delayed because of the pure delay function e^{-sT_i}. Therefore, when the velocity profile is convolved with a series of FIR filters, the filtered velocity profile will be smoothed

because of the increased order.

Two FIR filters in series will generate a velocity profile with trapezoidal acceleration constant jerk. For example, when a step-shaped command velocity profile with the command feedrate, F_t, for the length of time, T_v, is given, the filtered velocity is shown in Fig. 7. T_1 is the time constant of the first FIR filter and T_2 is the time constant of the second FIR filter. For the original step-shaped velocity pulse, the acceleration at starting time point (t=0) and ending time point (t=T_v) are theoretically infinite that definitely affect the tracking accuracy and may cause vibrations. In contrast, the acceleration and jerk of the filtered velocity pulse are limited. At the same time, the acceleration and jerk upper limits can be adjusted by tuning the time constants of the FIR filters [14].

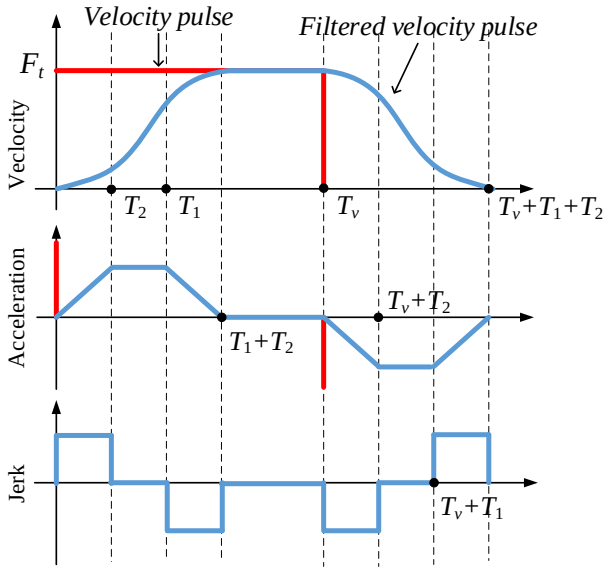

Fig. 7 Trapezoidal acceleration generated by FIR filtering.

The reference trajectory of each axis is individually filtered by the two FIR filters in series. Note that the time constants of the FIR filters for each axis are set to the same to ensure that each axis is driven synchronously. The filtered reference trajectories are regarded as the command trajectories in the MCS. Throughout this paper, the symbols with the superscript "*" represents a signal after the FIR filtering. This conventional Acc/dec filtering scheme for five-axis machining is shown in Fig. 8.

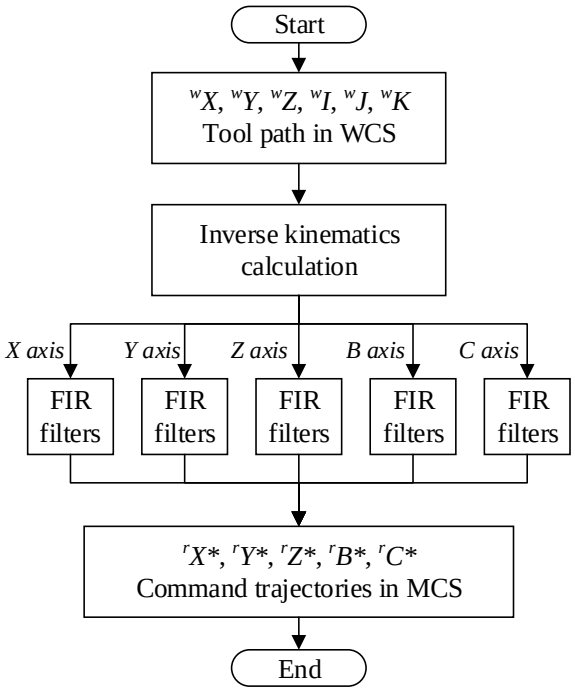

Fig. 8 Conventional Acc/dec FIR filtering scheme.

4.2 Contour error caused by tool path smoothing in the machine coordinate system

The Acc/dec smoothing by Eq. (3) inevitably introduces a delay to each axis. However, when two or three linear axes are driven synchronously for a straight command path, the delayed position is always on the command line, and thus it does not introduce any contour error, as long as the time constants are the same for all the axes. For a circular path, it is well known that the position delay introduces a uniform contour error in the radial direction. When the machine's dynamics is included, it requires numerical optimization of command trajectories or cross-coupling feedback control to reduce the contour error, which have been studied by many researchers [23, 24], but this paper only considers the delay introduced by the Acc/dec filtering.

For five-axis operation, the finished workpiece geometry is determined by the contour error in the WCS. No contour error in the MCS does not guarantee no contour error in the WCS, due to the delay in the angular position of rotary axes. When the smoothed reference trajectories in the MCS for *X*-, *Y*-, *Z*-, *B*-, and *C*-axes are given by $^{r}X^{*}(j)$, $^{r}Y^{*}(j)$, $^{r}Z^{*}(j)$, $^{r}B^{*}(j)$, $^{r}C^{*}(j)$, (j=1, ..., N), the tool path in the WCS has no contour error when the following condition is met:

$$ {}^{w}\boldsymbol{T}_{r} \times \begin{bmatrix} {}^{r}X^{*}(j) \\ {}^{r}Y^{*}(j) \\ {}^{r}Z^{*}(j) \end{bmatrix} = \begin{bmatrix} {}^{w}X^{*}(j) \\ {}^{w}Y^{*}(j) \\ {}^{w}Z^{*}(j) \end{bmatrix} \subseteq \left\{ \begin{bmatrix} {}^{w}X(j) \\ {}^{w}Y(j) \\ {}^{w}Z(j) \end{bmatrix} \right\}, \qquad j = 1, 2, \cdots, N \quad , \tag{4} $$

where $^{w}\boldsymbol{T}_{r}$ is the transformation matrix from the WCS to the MCS and is given by

$$ {}^{w}\boldsymbol{T}_{r} = \left(R_b\left(-{}^{r}B^{*}(j)\right) \cdot R_c\left(-{}^{r}C^{*}(j)\right)\right)^{-1} \quad , \tag{5} $$

and $R_b(b)$ and $R_c(c) \in \Re^{3*3}$ represent rotation matrices around Y- and Z-axes, respectively, by the angle b and c. In Eq. (5), the symbol "$\subseteq$" represents that the point in the left-hand side is included in the trajectory given by interpolating a set of points in the right-hand side.

Considering that the reference trajectory of each axis is filtered individually, it is difficult to ensure that the tool-tip position under the command trajectories control is still on the ideal tool path in the WCS. In Fig. 9, UV represents a reference trajectory in the MCS. The [X, Y, Z] position of a point on this trajectory is given by $\boldsymbol{P}(j)$: $[{}^{r}X(j), {}^{r}Y(j), {}^{r}Z(j)]$ with the corresponding rotary axis angular positions $\boldsymbol{R}(j)$: $[{}^{r}B(j), {}^{r}C(j)]$. Suppose that this point, $\boldsymbol{M}(j)$: $[\boldsymbol{P}(j), \boldsymbol{R}(j)]$, corresponds to the point $[{}^{w}X(j), {}^{w}Y(j), {}^{w}Z(j)]$ in the WCS.

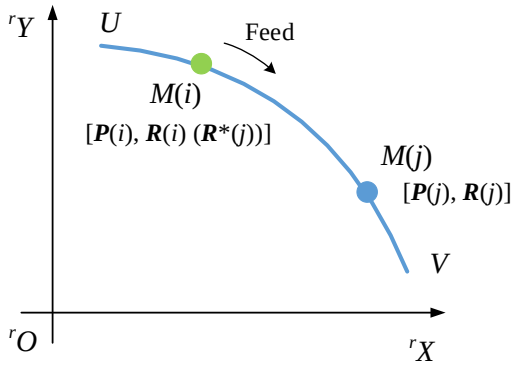

Fig. 9 Reference trajectory in the MCS.

Considering the delay caused by the FIR filters, the actual rotary axes positions corresponding to $M(j)$ are denoted by $\boldsymbol{R}^{*}(j)$: $[{}^{r}B^{*}(j), {}^{r}C^{*}(j)]$. On this UV trajectory, there must be a point, $M(i)$, at which the corresponding rotary axes position $\boldsymbol{R}(i)$ is equal to $\boldsymbol{R}^{*}(j)$. If the delayed linear axes position $\boldsymbol{P}^{*}(j)$: $[{}^{r}X^{*}(j), {}^{r}Y^{*}(j), {}^{r}Z^{*}(j)]$ is equal to $\boldsymbol{P}(i)$: $[{}^{r}X(i), {}^{r}Y(i), {}^{r}Z(i)]$ corresponding to $M(i)$, there will be no contour error. However, since the reference trajectory of each axis is filtered in the MCS, the actual delayed linear axes position $\boldsymbol{P}^{*}(j)$ in the MCS should be roughly on the line tangential to the path UV at point $M(j)$ as shown in Fig. 10 (the filtered position, $P^{*}(j)$, may be slightly displaced to the direction normal to this tangential line due to the delay causing the radial error in circular interpolation). The difference between the actual delayed position $M^{*}(j)$ and the desired delayed position $M(i)$ cause the contour error.

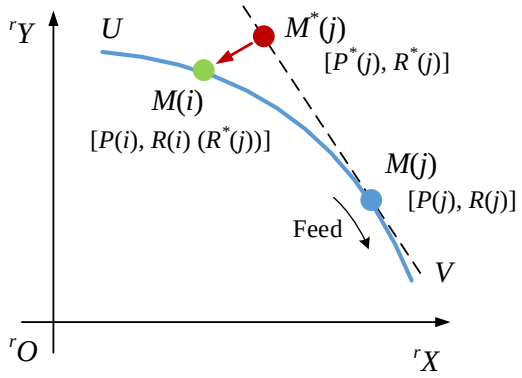

Fig. 10 Contour error caused by tool path filtering in MCS.

4.3 Analytical formulation of contour error in the proposed test

For the tool path designed in Fig. 1, the kinematics transformation from the TCP positions in the WCS to the reference trajectories in the MCS is expressed as below:

$$\begin{cases} {}^{r}X(j) = {}^{w}X(j)\cos\left({}^{r}C(j)\right) + {}^{w}Y(j)\sin\left({}^{r}C(j)\right) \\ {}^{r}Y(j) = -{}^{w}X(j)\sin\left({}^{r}C(j)\right) + {}^{w}Y(j)\cos\left({}^{r}C(j)\right) \end{cases}. \tag{6}$$

This section analytically formulates the contour error in the proposed machining test, when the conventional smoothing method, depicted in Fig. 8, is applied. Since the convolution processing can be separated ($E^*(F+G)=E^*F+E^*G$), the reference trajectory of X- and Y-axis can be considered separately. First, separate ${}^{r}X$ and ${}^{r}Y$ into the following two terms, i.e. ${}^{r}X(j)=S_{X1}(j)+S_{X2}(j)$, ${}^{r}Y(j)=S_{Y1}(j)+S_{Y2}(j)$, with:

$$\begin{cases} S_{X1} = {}^{w}X_0\cos(\omega_C t) \\ S_{X2} = Ft\sin(\omega_C t) \\ S_{Y1} = -{}^{w}X_0\sin(\omega_C t) \\ S_{Y2} = Ft\cos(\omega_C t) \end{cases}. \tag{7}$$

When one FIR filter with the time constant T_1, given in Eq. (3), is applied to Eq. (7), each of the filtered commands are calculated as follows:

$$\begin{cases} S^*_{X1} = \dfrac{2\,{}^{w}X_0 \sin\left(\dfrac{\omega_C T_1}{2}\right)\cos\left[\dfrac{\omega_C}{2}(2t-T_1)\right]}{\omega_C T_1} \\ S^*_{X2} = \dfrac{F\left\{-\sin\left[\omega_C(t-T_1)\right]+\omega_C(t-T_1)\cos\left[\omega_C(t-T_1)\right]+\sin(\omega_C t)-\omega_C t\cos(\omega_C t)\right\}}{{\omega_C}^2 T_1} \\ S^*_{Y1} = \dfrac{-2\,{}^{w}X_0 \sin\left(\dfrac{\omega_C T_1}{2}\right)\sin\left[\dfrac{\omega_C}{2}(2t-T_1)\right]}{\omega_C T_1} \\ S^*_{Y2} = \dfrac{F\left\{-\cos\left[\omega_C(t-T_1)\right]-\omega_C(t-T_1)\sin\left[\omega_C(t-T_1)\right]+\cos(\omega_C t)+\omega_C t\sin(\omega_C t)\right\}}{{\omega_C}^2 T_1} \\ {}^{r}C^* = \omega_C\left(t-\dfrac{T_1}{2}\right) \end{cases} . \quad (8)$$

Assuming that $\omega_c T_1/2$ is sufficiently small, the output commands are approximated as follows:

$$\begin{cases} S^*_{X1} = G_{T_1,1}\,{}^{w}X_0 \cos\left[\omega_C\left(t-\dfrac{T_1}{2}\right)\right] \\ S^*_{X2} = G_{T_1,2}F(t-T_1)\sin(\omega_C t) \\ S^*_{Y1} = -G_{T_1,1}\,{}^{w}X_0 \sin\left[\omega_C\left(t-\dfrac{T_1}{2}\right)\right] \\ S^*_{Y2} = G_{T_1,2}F(t-T_1)\cos(\omega_C t) \end{cases} , \quad (9)$$

where

$$\begin{cases} G_{T1,1} = \dfrac{\sin\left(\dfrac{\omega_C T_1}{2}\right)}{\dfrac{\omega_C T_1}{2}} \\ G_{T1,2} = \dfrac{\sin(\omega_C T_1)}{\omega_C T_1} \end{cases} . \quad (10)$$

$G_{T1,1}$ and $G_{T1,2}$ can be approximated by polynomial expansion as below:

$$\begin{cases} G_{T1,1} = 1 - \dfrac{\left(\dfrac{\omega_C T_1}{2}\right)^2}{3!} + \dfrac{\left(\dfrac{\omega_C T_1}{2}\right)^4}{5!} + \cdots \\ G_{T1,2} = 1 - \dfrac{(\omega_C T_1)^2}{3!} + \dfrac{(\omega_C T_1)^4}{5!} + \cdots \end{cases} . \quad (11)$$

When the second FIR filter with the time constant T_2 is applied, the formulation above is repeated. The final commands filtered by two FIR filters in series are calculated as below:

$$\begin{cases} {}^{r}X^{*} = G_{T1,1}G_{T2,1}\,{}^{w}X_0 \cos\left[\omega_C\left(t-\dfrac{T_1}{2}-\dfrac{T_2}{2}\right)\right] + G_{T1,2}G_{T2,2}F(t-T_1-T_2)\sin(\omega_C t) \\ {}^{r}Y^{*} = -G_{T1,1}G_{T2,1}\,{}^{w}X_0 \sin\left[\omega_C\left(t-\dfrac{T_1}{2}-\dfrac{T_2}{2}\right)\right] + G_{T2,2}G_{T2,2}F(t-T_1-T_2)\cos(\omega_C t) \end{cases}, \tag{12}$$

where

$$\begin{cases} G_{T2,1} = \dfrac{\sin\left(\dfrac{\omega_C T_2}{2}\right)}{\dfrac{\omega_C T_2}{2}} \\ G_{T2,2} = \dfrac{\sin(\omega_C T_2)}{\omega_C T_2} \end{cases}. \tag{13}$$

In the proposed test, the position error in the *X*-direction of the WCS defines the contour error of the finished test piece (see Fig. 1a). Therefore, the contour error is given by:

$$\Delta\,{}^{w}X = \left(1-G_{T1,1}G_{T2,1}\right){}^{w}X_0 + G_{T1,2}G_{T2,2}F\left(t-T_1-T_2\right)\sin\left[\frac{\omega_C}{2}\left(T_1+T_2\right)\right]. \tag{14}$$

Note that the velocity of *C*-axis is reversed at the middle position of the tool path, in other words, ω_C is a positive constant before this point, and is a negative constant before this point. According to the definitions in Eqs. (11) and (13), this does not change $G_{T1,1}$, $G_{T1,2}$, $G_{T2,1}$, and $G_{T2,2}$. It only changes the sign of the 2nd term in Eq. (14). As a result, the contour error in Eq. (14) shows a step at the reversal point. The size of the step depends on F, $G_{T1,2}$, and $G_{T2,2}$.

4.4 Improved tool path smoothing method

In this section, an improved tool path smoothing method is proposed. In the proposed tool path smoothing method, the tool path is firstly smoothed in the WCS along the feed direction, and then the command trajectory of each axis is obtained by solving the inverse kinematics calculation based on the filtered trajectory in the WCS. As reviewed in Section 1, some researchers [18-22] adopted essentially the same scheme. The entire process of the proposed tool path smoothing method is shown in Fig. 11.

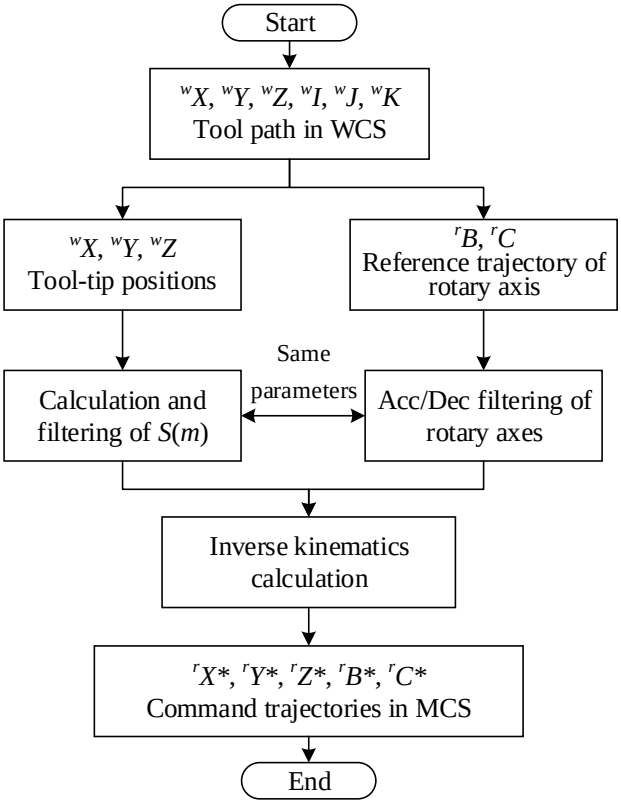

Fig. 11 Tool path smoothing on trajectory.

The smoothing by the FIR filter, Eq. (3), inevitably introduces a delay. Even when only *X*-, *Y*-, and *Z*-axes are involved, it causes the contour error. It is well known [15] that it causes 1) uniform radial error in circular interpolation, and 2) contour error at corners. To avoid it, the application of the Acc/dec filtering on the trajectory, not to each axis, has been proposed and implemented in commercial CNC systems (it is referred to as "Acc/dec filtering before interpolation" in some commercial CNC systems). In CNC systems, the Acc/dec filtering can be conducted before interpolation and after interpolation. The Acc/dec filtering after interpolation smooths the reference trajectory of each axis output by the tool path interpolation separately. The Acc/dec filtering before interpolation controls the feed rate directly and does not affect the position accuracy of the interpolation. For three linear axes, however, the application of Acc/dec before interpolation is not essential. The uniform radial error in circular interpolation can be compensated typically by a feed forward controller [25]. The contour error at corners can be reduced by various corner blending schemes [10-17] without explicitly applying this concept. On the other hand, in order to smooth the tool path in the workpiece coordinate system, the Acc/dec before interpolation has to be implemented, like the researches in [18-22]. The Acc/dec filtering on the trajectory is essential to eliminate the contour error, in five-axis interpolation. This paper clarifies it.

The detailed algorithm, depicted in Fig. 11, is described below.

(1) Acc/dec filtering on trajectory

Assume that the discrete tool-tip positions in the WCS are represented as $\boldsymbol{T}(j)$: $[{}^{w}X(j), {}^{w}Y(j), {}^{w}Z(j)]$ (j=1, …, N). Assume that the accumulated length of the line segments to the current tool position $\boldsymbol{T}(j)$, represented as $S(j)$, is given by (see Fig. 12):

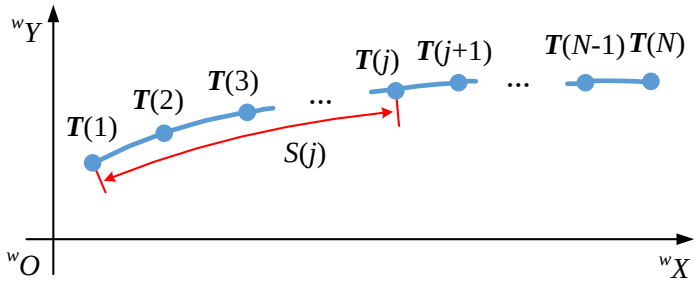

Fig. 12 Tool path distance and tool-tip positions.

$$S(j) = \sum_{m=2}^{j} \|\boldsymbol{T}(m-1)\boldsymbol{T}(m)\|, \quad j = 1,2,\cdots,N \quad , \tag{15}$$

where $\|\boldsymbol{T}(j\text{-}1)\ \boldsymbol{T}(j)\|$ represents the path length between the points $\boldsymbol{T}(j\text{-}1)$ and $\boldsymbol{T}(j)$. When the reference TCP trajectory in the WCS is given by $[{}^{w}X(j), {}^{w}Y(j), {}^{w}Z(j)]$ (j=1, …, N), it is first converted to S(j) by Eq. (15). Then, the profile of the derivative of S(j) is smoothed by applying two FIR filters (Eq. (3)). For example, when the feedrate on the trajectory $\dot{S}(j)$ is constant, the filtered velocity profile on the trajectory, $\dot{S}^{*}(j)$, and the filtered trajectory of the accumulated path length, $S^{*}(j)$, are given as illustrated in Fig. 13.

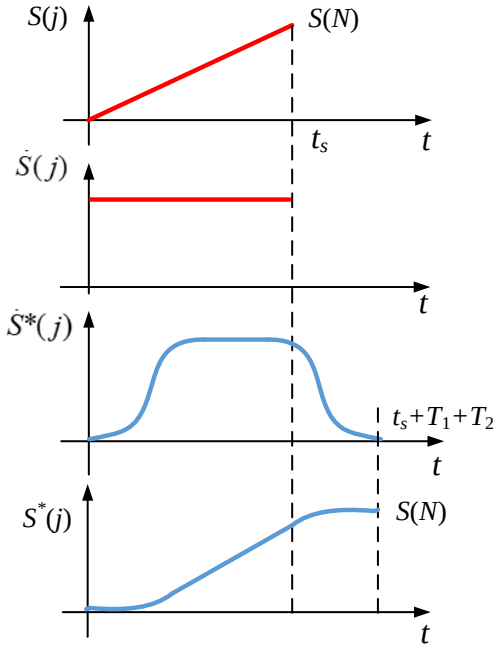

Fig. 13 Tool path smoothing on trajectory.

When the filtered tool path distance $S^{*}(j)$ is obtained, the corresponding tool-tip positions, $[{}^{w}X^{*}(j), {}^{w}Y^{*}(j), {}^{w}Z^{*}(j)]$

(j=1, …, N), can be calculated by interpolating $\boldsymbol{T}(j)$ (j=1, ..., N) with $S^*(j)$. The tool orientation in the WCS, denoted by [${}^wI(j)$, ${}^wJ(j)$, ${}^wK(j)$], is associated with each command position, $\boldsymbol{T}(j)$. It should be smoothed in the same manner as [${}^wX(j)$, ${}^wY(j)$, ${}^wZ(j)$], by interpolating [${}^wI(j)$, ${}^wJ(j)$, ${}^wK(j)$] with the smoothed $S^*(j)$. Denote the smoothed trajectory of tool orientation in the WCS by [${}^wI^*(j)$, ${}^wJ^*(j)$, ${}^wK^*(j)$].

(2) Inverse kinematics calculation based on smoothed trajectories

The inverse kinematics calculation is performed after the tool path smoothing. By solving the inverse kinematic problem, the smoothed reference trajectory for B- and C-axes, ${}^rB^*(j)$ and ${}^rC^*(j)$ can be calculated from [${}^wI^*(j)$, ${}^wJ^*(j)$, ${}^wK^*(j)$]. Then, the reference trajectories for X-, Y-, and Z- axes can be calculated by converting the smoothed trajectory in the WCS, [${}^wX^*(j)$, ${}^wY^*(j)$, ${}^wZ^*(j)$], to the MCS by Eq. (2).

4.5 Simulation

To further illustrate the influence of the smoothing in the MCS in the proposed machining test, in this section, the simulation of the contour error under the influence of five-axis tool path smoothing is conducted using two FIR filters in series. The time constants T_1 and T_2 of the two FIR filters in series are set as 0.1 s and 0.064 s, respectively. As in many commercial CNC systems, it is first converted to the MCS and then filtered as shown in Fig. 8. Then, to calculate the contour error, the filtered reference trajectories for X, Y and C axes, [${}^rX^*(j)$, ${}^rY^*(j)$, ${}^rZ^*(j)$], are converted to the WCS by inversely solving Eq. (2). The filtered TCP position in the WCS is represented by [${}^wX^*(j)$, ${}^wY^*(j)$]. The contour error is given by:

$$\Delta {}^wX(j) = {}^wX^*(j) - {}^wX(j) \quad . \tag{16}$$

The filtered reference trajectories for X-, Y- and C-axes, ${}^rX^*$, ${}^rY^*$, and ${}^rC^*$, are shown in Fig. 14a. The simulated contour error, Δ^wX, is shown in Fig. 14b. The X-position of the reference trajectory in the WCS is 121.286 mm but is shown as zero in Fig. 14b. The tool paths under different feedrates (F=9180, 7120, and 3060 mm/min) are simulated in Fig. 14b. For the tool path under feedrate 9180 mm/min, the maximum contour error even exceeds 0.3 mm. Though the defined feedrate in the WCS is high, the size and shape of the contour error is unacceptable for high-precision five-axis machining. For comparison, command trajectories for X, Y, and C-axes under the proposed tool path smoothing method shown in Fig. 9 are simulated as shown in Fig. 14a. The corresponding simulated contour error is shown in Figure 14b. The simulation results show that the proposed tool path smoothing method completely eliminates the contour error.

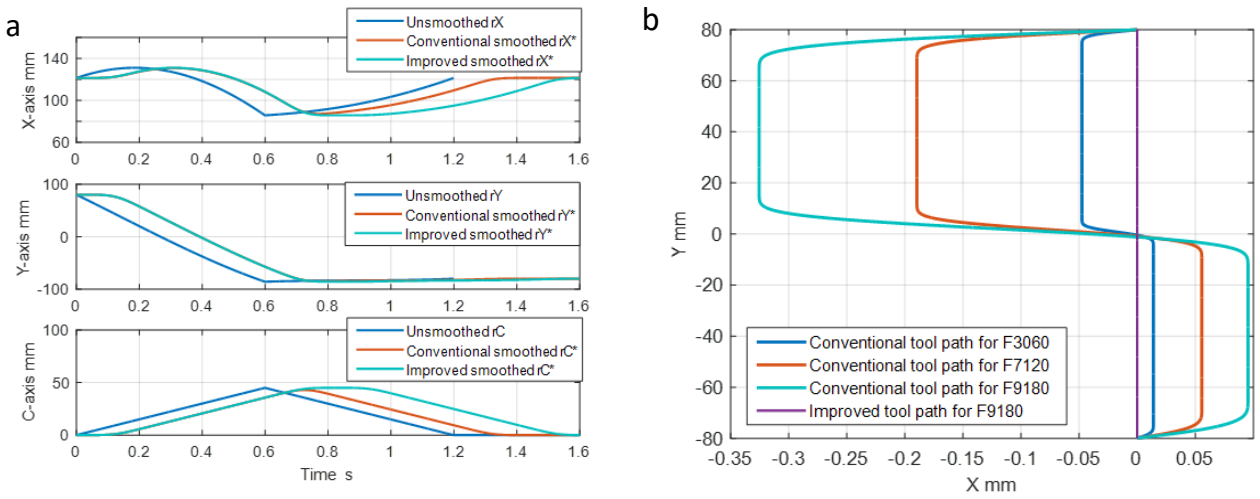

Fig. 14 Trajectories of axes and tool path under the conventional tool path smoothing method (a) filtered trajectories under the feedrate 9180 mm/min in MCS, (b) simulated tool paths in WCS.

Remark: The simulation result in Fig. 14 and experimental result in Figs. 4 and 6 show similar step-shaped contour error, but the size of the contour errors is different. The smoothing filter in the simulation model consists of two FIR filters with fixed time constants, T_1 and T_2 (see Eq. (3)). On the other hand, in Fanuc 30i controller, according to its manual, the steady-state acceleration (see Fig. 7) is constant regardless of the command feedrate, unless it exceeds the prescribed limit. This suggests that the time constants of the smoothing filter are not fixed. More detailed formulation of the smoothing filter in this controller is not disclosed. This discrepancy of the smoothing filter used in the simulation model explains the difference between simulated and experimental contour errors.

5. Discussion: extended machining test to observe contour error near the singularity

Although some researchers have presented that the Acc/dec smoothing in the MCS causes a contour error in the WCS, many commercial five-axis machine tool controllers still adopt the Acc/dec filtering in the MCS, mainly for the following two reasons: 1) the Acc/dec smoothing in the MCS cannot cause the singularity issue. Care must be taken to avoid the singularity, when the Acc/dec smoothing is applied in the WCS. 2) It is just computationally less stringent by avoiding spherical interpolation and inverse kinematics calculations. By performing the present machining test, however, a user can clearly observe that the Acc/dec smoothing in the MCS can result in a significant geometric error, up to 0.14 mm as shown in Fig. 6, of the finished test piece surface. A user would understand the necessity of the Acc/dec smoothing in the WCS. This is one of the major contributions of this paper.

A significant influence of the Acc/dec smoothing in the MCS on the contour error can be observed not only in the present machining test. It is often observed when the machine is operated near the five-axis singularity. An illustrative example will be presented. Figure 15 shows a machining test procedure. In the WCS, A surface tilted by 45° from the XZ

plane is machined by using a ball end mill. In the first half of each path, the tool is tilted by 0.1° around Y-axis, and is fed to the X-direction. In the second half, the tool is tilted by 0.1° around X-axis, and is fed to the X-direction. On the centerline (X=0), the tool changes its orientation. Assuming the machine has the C-axis (around Z-axis) and B-axis (around Y-axis), although the change in the tool orientation is very small (-0.1° around Y-axis and 0.1° around X-axis), the C-axis must rotate by 90°. This is due to the five-axis singularity when the tool is parallel to the C-axis of rotation. Figure 16 shows the command trajectories in the MCS for X, Y, and C-axes. The singularity causes a sudden change in X, Y and C position to slightly change the tool orientation in the WCS.

This causes a large contour error. Figure 17 shows the contour error, the (X, Y, Z) position trajectory, measured by linear encoders and recorded by Servoguide in an experiment, and converted to the WCS in the same manner as in Fig. 4b. The maximum contour error was 0.17 mm. This resulted in a clear “bump” on the nominally flat finished surface. The major cause is the same as the one discussed in Section 4.2; the Acc/dec smoothing in the MCS. The contribution of the feedback control transient dynamics is minor.

Further analysis of this machining test is left for our future research. However, this illustrative example shows that a potentially large contour error, caused by the Acc/dec smoothing in the MCS, can occur frequently in the five-axis machining, when the tool orientation is near the singularity (i.e. parallel to C-axis). The present machining tests (Figs. 1 and 15) help a user to recognize a potentially critical influence of the Acc/dec smoothing in the MCS on the contour error. This is a major contribution of this paper.

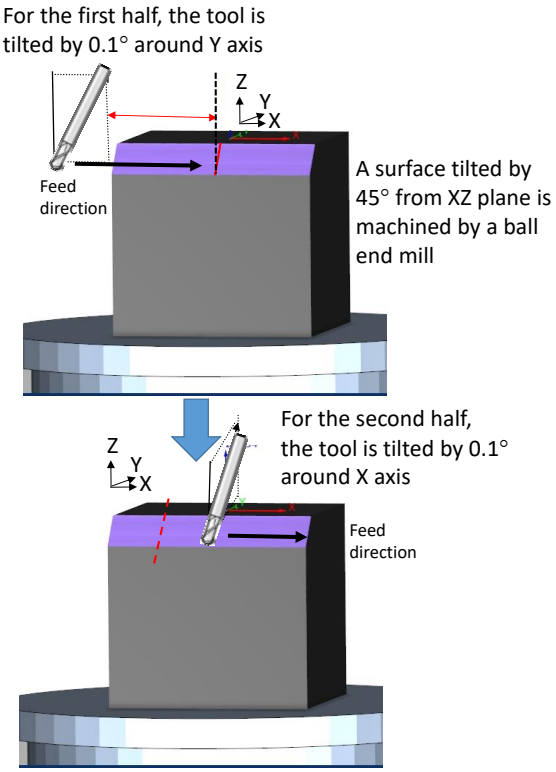

Fig. 15 Machining test procedure; the tool’s feed and orientation in the WCS.

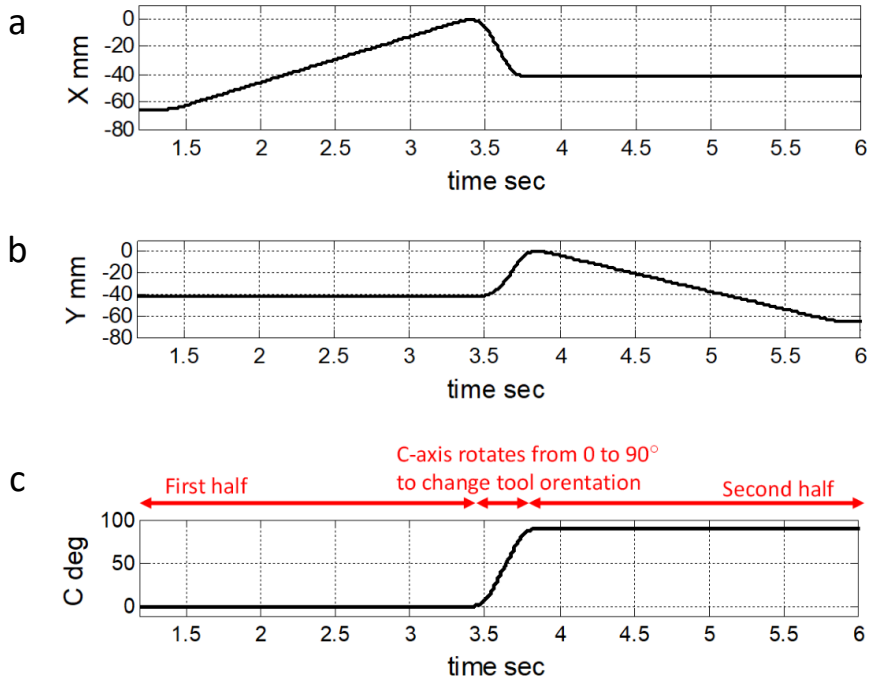

Fig. 16 Recorded trajectories in the MCS measured by linear encoder. a) X-axis, b) Y-axis, c) C-axis.

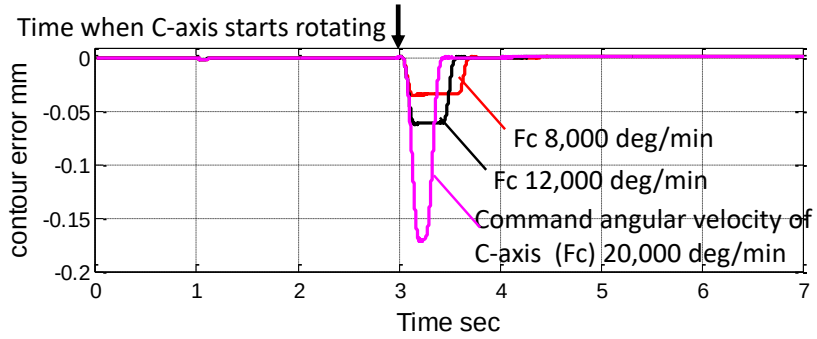

Fig. 17 Recorded contour error profile measured by linear encoders converted to the WCS.

6. Conclusion

The contributions of this study are summarized below:

- This paper proposed a machining test with the main objective to quantitatively evaluate the influence of the synchronization error of rotary and linear axes on the machined surface. The experiment showed that the step-shaped geometric error of the finished surfaces in the proposed machining test was as at maximum 0.16 mm under the conventional smoothing in a commercial CNC system, which is significantly larger than the influence of other typical geometric errors of a five-axis machine tool.
- In five-axis operations, many commercial CNC systems apply a smoothing Acc/dec filter to command trajectories in the MCS. This paper clarified that it can cause a significant contour error due to the delay introduced by the filter.

- This paper also clarifies that the command trajectory must be smoothed in the WCS to eliminate this contour error, i.e. the velocity profile on the TCP trajectory in the WCS should be first filtered and then the command trajectory of each axis in the MCS is obtained by solving the inverse kinematics calculation. Its effectiveness was verified by simulation, but experimental validation was not presented, since it was difficult for us to implement it on a commercial CNC system. The similar smoothing in the WCS is proposed in some other academic studies [18-22], in which their focus is on the corner blending in the WCS and the machining efficiency improvement. But the CNC users and builders do not clearly see how significant this influence of the conventional smoothing in the MCS can be on the machining accuracy, which we claim is the main reason why this influence is overlooked. The proposed machining test enables a user to observe its influence.

Reference

1. Ibaraki S, Knapp W. (2013) Indirect measurement of volumetric accuracy for three-axis and five-axis machine tools: a review. International Journal of Automation Technology, 6(2), 110-124.
2. ISO 10791-6. (2014) Test conditions for machining centres — Part 6: Accuracy of speeds and interpolations.
3. Tsutsumi M, Saito A. (2003) Identification and compensation of systematic deviations particular to 5-axis machining centers. International Journal of Machine Tools and Manufacture, 43(8), 771-780.
4. Hong C, Ibaraki S, Oyama C. (2012) Graphical presentation of error motions of rotary axes on a five-axis machine tool by static r-test with separating the influence of squareness errors of linear axes. International Journal of Machine Tools and Manufacture, 59, 24-33.
5. Ding W, Zhu X, Huang X. (2016) Effect of servo and geometric errors of tilting-rotary tables on volumetric errors in five-axis machine tools. International Journal of Machine Tools and Manufacture, 104, 37-44.
6. Wang W, Jiang Z, Li Q, Tao W. (2015) A new test part to identify performance of five-axis machine tool-Part II validation of S part. The International Journal of Advanced Manufacturing Technology, 79(5-8), 739-756.
7. Cripps RJ, Cross B, Hunt M, Mullineux G. (2017) Singularities in five-axis machining: cause, effect and avoidance. International Journal of Machine Tools and Manufacture, 116, 40-51.
8. Jeon JW, Ha YY. (2000) A generalized approach for the acceleration and deceleration of industrial robots and CNC machine tools. Industrial Electronics IEEE Transactions on industrial Electronics, 47(1), 133-139.
9. Erkorkmaz K, Altintas Y. (2001) High speed CNC system design. part i: jerk limited trajectory generation and quintic spline interpolation. International Journal of Machine Tools and Manufacture, 41(9), 1323-1345.
10. Sencer B, Ishizaki K, Shamoto E. (2015) A curvature optimal sharp corner smoothing algorithm for high-speed feed motion generation of NC systems along linear tool paths. The International Journal of Advanced Manufacturing Technology, 76(9-12), 1977-1992.
11. Essid M, Gassara B, Baili M, Hbaieb M, Dessein G, Saï WB. (2019) Analytical modeling of the CNC machine axis motion in high-speed milling with local smoothing. The International Journal of Advanced Manufacturing Technology, 105(1-4), 457-470.
12. Rymansaib Z, Iravani P, Sahinkaya MN. (2013, July) Exponential trajectory generation for point to point motions. In 2013 IEEE/ASME international conference on advanced intelligent mechatronics, 906-911.
13. Chen CS, Lee AC. (1998) Design of acceleration/deceleration profiles in motion control based on digital fir filters. International Journal of Machine Tools and Manufacture, 38(7), 799-825.
14. Biagiotti L, Melchiorri C. (2012). FIR filters for online trajectory planning with time-and frequency-domain specifications. Control Engineering Practice, 20(12), 1385-1399.
15. Tajima S, Sencer B, Shamoto E. (2018) Accurate interpolation of machining tool-paths based on FIR filtering. Precision Engineering, 52, 332-344.
16. Tajima S, Sencer B. (2017) Global tool-path smoothing for CNC machine tools with uninterrupted acceleration. International Journal of

Machine Tools and Manufacture, 121, 81-95.

17. Hayasaka T, Minoura K, Ishizaki K, Shamoto E, Sencer B. (2019) A lightweight interpolation algorithm for short-segmented machining tool paths to realize vibration avoidance, high accuracy, and short machining time. Precision Engineering, 59, 1-17.
18. Sencer B, Altintas Y, Croft E. (2008) Feed optimization for five-axis CNC machine tools with drive constraints. International Journal of Machine Tools and Manufacture, 48(7-8), 733-745.
19. Huang X, Zhao F, Tao T, Mei X. (2020) A novel local smoothing method for five-axis machining with time-synchronization feedrate scheduling. IEEE Access, 8, 89185-89204.
20. Hu Q, Chen Y, Jin X, Yang J. (2020) A real-time C3 continuous tool path smoothing and interpolation algorithm for five-axis machine tools. Journal of Manufacturing Science and Engineering, 142, 041002.
21. Jiang Y, Han J, Xia L, Lu L, Tian X, Liu H. (2020) A decoupled five-axis local smoothing interpolation method to achieve continuous acceleration of tool axis. The International Journal of Advanced Manufacturing Technology, 111, 449–470.
22. Tajima S, Sencer B. (2019) Accurate real-time interpolation of 5-axis tool-paths with local corner smoothing. International Journal of Machine Tools and Manufacture, 142, 1-15.
23. Koren Y. (1980) Cross-coupled biaxial computer control for manufacture systems, ASME Journal Of Dynamic System, Measurement, and Control 102, 265–272.
24. Shih YT, Chen CS, Lee AC. (2002) A novel cross-coupling control design for Bi-axis motion. International Journal of Machine Tools and Manufacture, 42(14), 1539-1548.
25. Ang WT, Khosla PK, Riviere CN. (2007) Feedforward controller with inverse rate-dependent model for piezoelectric actuators in trajectory-tracking applications. IEEE/ASME Transactions on Mechatronics, 12(2), 134-142.